NASA Technical Memorandum 89132

STATIC AEROELASTIC EFFECTS ON THE
FLUTTER OF A SUPERCRITICAL WING

E. Carson Yates, Jr., and Li-Chuan Chu

MARCH 1987

STATIC AEROELASTIC EFFECTS ON THE FLUTTER OF A SUPERCRITICAL WING

E. Carson Yates, Jr.
Chief Scientist
Loads and Aeroelasticity Division
NASA Langley Research Center
Hampton, Virginia 23665-5225

Li-Chuan Chu
Research Engineer
PRC Kentron Corporation
Hampton, Virginia 23666
U. S. A.

SUMMARY

It is well known that wings with supercritical airfoils generally have lower transonic flutter speeds than similar wings with conventional airfoils and that small increases in angle of attack from zero and the accompanying static aeroelastic deformations have further detrimental effects on transonic flutter. This paper presents the results of an effort to calculate the effects of angle of attack and the associated aeroelastic deformation on the flutter of a highly swept supercritical wing (TF-8A) by use of the modified strip analysis employed in previous studies of this wing. The spanwise distributions of steady-state section lift-curve slope and aerodynamic center required as input for these calculations were obtained from static aeroelastic calculations for the wing by use of the FLO22 transonic code and an assumed dynamic pressure. The process is iterative so that flutter can be obtained at the same dynamic pressure as that used to calculate the statically deformed shape and loading about which the flutter oscillation occurs (matched conditions). The results of this investigation show that the unconventional backward turn of the transonic dip in the experimental flutter boundary for angles of attack greater than zero is caused by variations in mass ratio and not by static aeroelastic deformation, although inclusion of the latter appears to be required for quantitative accuracy in the calculations. For the very high subsonic Mach numbers of this investigation, however, quantitative accuracy will also require inclusion of viscous effects on shock strength and location.

SYMBOLS

$a_{c,n}$ nondimensional distance from midchord to section aerodynamic center measured perpendicular to elastic axis, positive rearward, fraction of semichord

b semichord of wing measured perpendicular to elastic axis at station n

b_r semichord of wing at spanwise reference station ($n = 0.75$)

C_{L_0} wing lift coefficient at $\alpha = 0$

C_{L_α} wing lift-curve slope

C_ℓ section lift coefficient for a section perpendicular to elastic axis

$C_{\ell_\alpha,n}$ section lift-curve slope for a section perpendicular to elastic axis

C_m section-pitching moment coefficient referred to midchord for a section perpendicular to elastic axis

k reduced frequency, $b_r\omega/V\cos\Lambda_{ea}$

M freestream Mach number

m_r mass of wing per unit span at spanwise reference station ($n = 0.75$)

q freestream dynamic pressure

V freestream speed

V_I flutter-speed index, $\dfrac{V}{b_r\omega_r\sqrt{\mu_r}}$

α angle of attack at wing root

n nondimensional coordinate measured from wing root along elastic axis, fraction of elastic axis length

Λ_{ea} sweep angle of elastic axis

μ_r mass ratio based on spanwise reference station ($\eta = 0.75$), $m_r/\pi\rho b_r^2$

ρ freestream density

ω circular frequency of vibration

ω_r reference frequency, frequency of first uncoupled torsional mode of wing

INTRODUCTION

It is well known that the use of supercritical airfoils, rather than conventional airfoils, can have adverse effects on the transonic flutter characteristics of lifting surfaces. The effects include reduction of transonic flutter speeds (refs. 1 to 3) and increased rate of degradation of flutter speed with small increases in angle of attack (refs. 4 and 5). In order to gain insight into these deleterious effects and the physical phenomena involved, a computational flutter study was conducted half a dozen years ago for a flutter model of the supercritical wing of the TF-8A airplane (fig. 1). Since adequate aerodynamic theories for three-dimensional unsteady transonic flow were not available, the modified strip analysis (refs. 6 to 12) was used. Spanwise distributions of steady-state section lift-curve slope and aerodynamic center, required as input to the flutter calculations, were obtained from wind-tunnel pressure measurements on another model of the same airplane.

The calculated flutter results compared well with experiments for 0° and 1° angles of attack but did not reproduce the drastic decline in transonic flutter speeds shown by the experiments at 2° and 3° angles of attack (ref. 5). The trends seemed to indicate, however, that the latter discrepancy was caused at least to some extent by the fact that the pressure model, from which the aerodynamic inputs were obtained, was two orders of magnitude stiffer than the flutter model and hence deformed statically much less than the flutter model.

The present investigation was initiated to address that problem. The same methodology is used except that the spanwise distributions of section lift-curve slope and aerodynamic center are obtained from static aeroelastic calculations for the flutter model employing the FLO22 full-potential code (ref. 13). Dynamic pressure is iterated between the aeroelastic calculation and the flutter calculation in order to obtain flutter at the same dynamic pressure as that used to calculate the static deformation and loading. The objective of this investigation is not to develop new methodology but to study the physical phenomena involved.

FLUTTER ANALYSIS METHOD

The modified strip analysis (ref. 6) is formulated for wing strips oriented normal to the elastic axis and is based on stripwise application of Theodorsen-type aerodynamics (ref. 14) in which the lift-curve slope of 2π and aerodynamic center at quarter chord are replaced, respectively, by the lift-curve slope and aerodynamic center for the same strip of the three-dimensional wing at the appropriate Mach number and angle of attack. The downwash collocation point, where the downwash induced by the aerodynamic load is set equal to the kinematic downwash, is modified accordingly. The aerodynamic admittance function (circulation function) is modified for compressibility by use of two-dimensional unsteady compressible-flow theory (ref. 15).

The simple example of section lift L on an unswept wing can be used to illustrate the changes to Theodorsen aerodynamics that are involved in the modified strip analysis.

For a three-dimensional wing in compressible steady flow, the section lift is given in terms of the section lift-curve slope $C_{\ell_{\alpha,n}}$ and the static angle of attack α or alternatively the downwash $Q=\alpha V$.

$$L = C_{\ell_{\alpha,n}} \alpha \frac{\rho}{2} V^2 (2b) = C_{\ell_{\alpha,n}} \rho V b Q$$

For two-dimensional incompressible oscillatory flow, the section lift as given by Theodorsen can be expressed in similar form.

$$L = 2\pi\rho VbQC + \text{noncirculatory terms}$$

Now, however, the lift-curve slope for two-dimensional incompressible flow is 2π, and the circulatory lift is multiplied by an aerodynamic admittance function (circulation function) $C(k)=F_I + iG_I$. The downwash Q is the unsteady downwash evaluated at the three-quarter-chord point which is the collocation point for induced and kinematic downwash in two-dimensional incompressible flow. Noncirculatory lift terms which have no counterpart for steady flow are also included.

For three-dimensional compressible oscillatory flow, the Theodorsen form of the expression is retained for the modified strip analysis

$$L = C_{\ell_{\alpha,n}} \rho V b Q C + \text{noncirculatory terms}$$

but with three modifications: (a) The lift-curve slope is no longer 2π but the value for the particular section of the three-dimensional wing at the particular Mach number, angle of attack, and other conditions being studied. (b) The downwash collocation point is no longer at three-quarter chord but is relocated to satisfy the trailing-edge condition for the particular section lift-curve slope and aerodynamic-center position involved. (c) The circulation function for incompressible flow is modified in magnitude only to account for compressibility.

$$C(k,M) = \sqrt{\frac{F_C^2 + G_C^2}{F_I^2 + G_I^2}} \; (F_I + iG_I) \sim \frac{F_C}{F_I} (F_I + iG_I)$$

where subscripts C and I indicate values for two-dimensional compressible and incompressible flow, respectively. Similar modifications are also made, of course, in the corresponding expression for section pitching moment (refs. 6 and 7). Note that no arbitrary user-selected parameters are included in the expressions in order to improve the agreement with experimental flutter data or with other calculations.

The modified strip analysis has consistently given good flutter results for a broad range of swept and unswept wings at speeds up to hypersonic (ref. 7), including effects of wing thickness (refs. 9 and 10) and angle of attack (ref. 11). In particular, this method which was developed in the mid 1950's (ref. 6) was used successfully in 1959 to calculate transonic flutter characteristics for some swept wings with conventional airfoils (ref. 8). In 1979, it was used to calculate transonic flutter of the present supercritical wing at essentially zero angle of attack with exceptionally good results (ref. 3). That study was extended in 1980 to include nonzero angles of attack (ref.5).

PREVIOUS FLUTTER CALCULATIONS FOR TF-8A WING

For Experiments in Freon-12

In the calculations for the TF-8A wing shown in figure 2 (from ref. 3), the required aerodynamic parameters were obtained from steady-state surface pressure measurements in the Langley 8-foot Transonic Tunnel (ref. 16). In the subsonic range, agreement between calculated and measured flutter boundaries is excellent. In the transonic range, a transonic dip is calculated which closely resembles the experimental one with regard to both shape and depth. However, the calculated dip occurs at about 0.04 Mach number lower than the experimental one. The reason for this difference is not known with certainty. There is some evidence, however, that indicates that the difference may be associated with model size relative to tunnel dimensions. The pressure model from which the aerodynamic coefficients were obtained for use in the flutter calculations was smaller relative to tunnel size than was the flutter model.

Note also that the experimental flutter data in figure 2 as well as the aerodynamic parameters used in the corresponding flutter calculations were obtained at essentially zero angle of attack. Consequently, the associated static aerodynamic loads and aeroelastic deformations were small and were not expected to influence flutter characteristics to any significant extent.

The experimental flutter data shown in figure 2 were obtained with Freon-12* gas used as test medium. Therefore, the associated values of mass ratio (fig. 3) were relatively low.

For Experiments in Air

The good results shown in figure 2 (from ref. 3) encouraged an extension of the study to examine the effects of angle of attack on flutter (ref. 5). The required aerodynamic parameters $C_{\ell\alpha,n}(\eta)$ and $a_{c,n}(\eta)$ were obtained from the same wind-tunnel pressure data as before, and representative values are shown in figures 4 and 5.

Figure 4 shows representative spanwise distributions of section lift-curve slope and aerodynamic center obtained from measured surface pressures at two subsonic Mach numbers. Nonlinearity with respect to angle of attack is minor at Mach number 0.25 but increases as Mach number rises to 0.80, especially in the aerodynamic center location. Note that the TF-8A wing was designed for an unusually high drag-rise Mach number (M=0.99).

As Mach number increases further, nonlinearity (as typified in fig. 5) becomes substantial and portends growing sensitivity of flutter speed to changes in angle of attack. Note, however, that the aerodynamic model on which the pressures were measured was two orders of magnitude stiffer than the flutter model in both bending and torsion. Consequently, aeroelastic deformation of the aerodynamic model was small, and the effects of angle of attack shown here are essentially aerodynamic (rather than aeroelastic) in origin.

---

* Freon is a registered trademark of E. I. DuPont de Nemours Co., Inc.

The corresponding flutter results for angles of attack from 0 deg to 3 deg are shown in figures 6(a) to 6(d) (from ref. 5). Note that the mass-ratio values shown on the figures for these experiments in air are considerably higher than those for the experiments in Freon-12 which were shown in figures 2 and 3.

At each Mach number for which the aerodynamic experiments were conducted (ref. 16), pressures on the wing surface were measured at two levels of freestream dynamic pressure, and both were used in the flutter calculations of reference 5 as indicated by the solid and dash lines in figures 6(a) to 6(d). Moreover, the Mach numbers for the aerodynamic experiments did not coincide with the experimental flutter Mach numbers. Therefore, no attempt was made to match experimental flutter conditions point for point with respect to Mach number and mass ratio. Instead, the flutter calculations were made only for the maximum and minimum experimental values of mass ratio at each angle of attack.

For $\alpha = 0$ (fig. 6(a)), static aeroelastic deformations of the flutter model were not significant, and the conventionally shaped experimental flutter boundary is reasonably well predicted by the calculated values which are about 6 percent conservative at $M = 0.85$ and a bit more so at the bottom of the transonic dip.

When α is increased to 1^0 (fig. 6(b)), the depth and location of the transonic dip are still adequately predicted, but the unconventional backward turn of the experimental boundary is not.

When α is further increased to 2^0 and 3^0 (figs. 6(c) and 6 (d), respectively), the backward turn of the experimental transonic flutter boundary becomes much more pronounced, and the bottom of the dip obviously drops drastically although the actual bottom is not defined by the available data points. The extent of this decline is not adequately predicted by the calculations. There is some evidence to indicate, however, that this discrepancy was caused at least to some extent by the fact that the pressure model, from which aerodynamic parameters were obtained for the flutter calculations, did not deform aeroelastically nearly as much as the flutter model did. Hence the aerodynamic parameters were not those relevant to the statically deformed wing shape about which the experimental flutter motion occurred. See reference 5 for more detailed discussion.

Experimental transonic flutter data for angles of attack up to 2.05 deg are presented in reference 17 for a high-aspect-ratio supercritical wing with, however, lower sweep angle and lower drag-rise Mach number than those for the TF-8A. The wing of reference 17 was provided some degree of flexibility in pitch, but the torsional stiffness of the wing itself appears to have been sufficiently high to prevent twisting deformations of significant magnitude. The measured transonic flutter boundary for that wing at 2.05 deg angle of attack is remarkably similar to the flutter boundary calculated for the TF-8A wing at 2 deg angle of attack using aerodynamic parameters obtained with the comparatively stiff pressure model of reference 16 (fig. 6(c)). The flutter boundaries for both wings show a relatively broad conventional-looking initial transonic dip followed by a steeper, narrower, deeper, and lower second dip. Second dips of this sort have been observed in wind-tunnel flutter-test results for other models under conditions for which static aeroelastic deformations would be expected to be mimimal (e.g., ref. 18).

Finally, it is illuminating to examine the variation of mass ratio with Mach number for the experimental flutter data shown in figures 6(a) to 6(c). On the curves of these parameters (fig. 7) the only firm values are those represented by the symbols which correspond to the "hard" flutter points in figures 6(a) to 6(c). The curves faired through the symbols in figure 7, however, are consistent with the curves faired through the "hard" flutter points in figures 6(a) to 6(c).

For $\alpha = 0$, the variation of mass ratio is moderate and of conventional form (compare fig. 3). For $\alpha = 1$ deg and especially for $\alpha = 2$ deg, on the other hand, the deep backward-turning transonic dips shown in figures 6(b) and 6(c) correspond to substantial increases in mass ratio. These wide excursions in mass ratio indicate that the experimental flutter boundaries follow substantially different tracks across the flutter-speed surface (defined by $V_I = f(M,\mu_r)$) for $\alpha = 0$, 1, and 2 degrees. The large values of mass ratio in themselves would produce low values of flutter-speed index. This point will be addressed subsequently in this paper. See also the more detailed discussion of the flutter-speed surface and the implications for flutter experiments and data interpretation in Appendix C of reference 10 and in reference 12.

PRESENT ANALYSIS

The inadequacy of the available experimental aerodynamic data for application to conditions involving significant static aeroelastic deformation of the flutter model led to the present study in which the required aerodynamic parameters were obtained from static aeroelastic calculations (fig. 8) incorporating FLO22 aerodynamics (ref. 13). Pressure distributions were thus computed for the aeroelastically deformed wing at a given Mach number, several angles of attack, and an initially chosen dynamic pressure. Since experimental flutter data were available, the Mach numbers and dynamic pressures were taken to be those for the measured flutter points. The calculated pressures were integrated to generate spanwise distributions of section lift and pitching-moment coefficients. These coefficients were then spline fitted as functions

of angle of attack, and the spline curves were analytically differentiated to produce section lift-curve slopes and moment-curve slopes (and hence aerodynamic centers) for the angles of attack at which the flutter data were measured. The spanwise distributions of section lift-curve slope and aerodynamic center were input to the modified strip analysis to generate generalized aerodynamic forces for use in the FAST flutter-analysis program (ref. 19). The resulting flutter dynamic pressure could then be used to modify the dynamic pressure input to the static aeroelastic calculation and the process iterated to produce flutter and static deformation (and associated pressure distributions) for the same (matched) dynamic pressure.

The FLO22 finite-difference code (ref. 13) implements a nonconservation form of the full potential equation. It was employed in this investigation because it had been previously incorporated into a static aeroelastic analysis (ref. 20) and previously used by the present first author in some unpublished calculations of the type presented here but for a different supercritical wing.

RESULTS AND DISCUSSION

For all of the flutter calculations made with aerodynamic parameters from FLO22, the Mach number, angle of attack and mass ratio for the experimental flutter points were essentially duplicated. As in reference 3 and 5, six measured natural modes of vibration were used in all flutter calculations. In figs. 9 and 10, the results are compared with the previously shown experimental flutter points and with the flutter boundaries calculated with the experimental aerodynamic parameters described previously (e.g., figs. 4 and 5; see also ref. 5). Note that the present calculations have been limited to the subsonic side of the transonic dip. Investigation of the subsonic side was considered to be sufficient to indicate the occurrence, character, and causes of the backward-turning transonic dip.

<u>Calculations for Design Shape of Wing</u>

An initial set of aerodynamic (FLO22) calculations was made for the wing deformed into its design shape and treated as rigid. The spanwise distributions of section lift-curve slope and aerodynamic center thus obtained were used in some initial flutter calculations. The resulting nondimensional flutter speeds V_I are represented by the diamond symbols in figs. 9 and 10. For zero angle of attack (fig. 9(a)), the calculated flutter speeds are in good agreement with experiment and differ very little from those obtained with the experimental aerodynamic parameters for (normally) the design shape. At $\alpha = 1$ deg (fig. 9(b)), the agreement is again good at the lowest experimental Mach number and mass ratio, but the calculated points become progressively unconservative as mass ratio increases to 547. It is important to note, however, that the backward turn of the flutter boundary is clearly indicated by the three calculated points, thus indicating that varying aeroelastic deformation is not essential to produce this behavior. Instead, the backward turn shown here is caused by the indicated variation in mass ratio. If the three calculated points are compared on the basis of a constant mass ratio, say $\mu_r = 450$. (results not shown), no backward turn appears. Results that are qualitatively similar to those in fig. 9(b) for $\alpha = 1$ deg are shown in fig. 9(c) for $\alpha = 2$ deg.

These progressively more unconservative predictions of flutter-speed index as mass ratio increases were anticipated from these calculations in which static aeroelastic deformation was neglected. Consider the experimental flutter boundary shown in figs. 9(c) and 10 for the flexible flutter model. As mass ratio increases, the flutter-speed index (and hence flutter dynamic pressure) decreases. As dynamic pressure decreases, static aeroelastic deformation (notably wing washout) diminishes, and section lift-curve slopes increase, especially over the outboard sections of the wing. As section lift-curve slopes increase, flutter dynamic pressure and flutter-speed index decrease. In other words, as mass ratio increases, diminishing static aeroelastic deformation of the flutter model contributes to lower flutter-speed index, and that effect is not included in the calculations for the rigid design shape (figs. 9(b) and (c) and fig. 10). Moreover, static loads and deformations and their effects should increase with increasing angle of attack, and the effects just described are indeed observed in figs. 9(a), (b), and (c) to become more pronounced as angle of attack increases. In fact, the effects of static deflection appear to be negligible at zero angle of attack (fig. 9(a)).

In fig. 10 the experimental and calculated transonic dips in fig. 9(c) have been enlarged and the calculations extended to show the bottom portion of the dip which has been calculated by use of the mass-ratio variation for $\alpha = 2$ deg shown in fig. 7. The latter, in turn, is consistent with the bottom portion of the dip faired through the experimental flutter points. These calculations for the rigid design shape show clearly that the unconventional backward-turning transonic flutter boundary is caused by variation in mass ratio and not by static aeroelastic deformation. Accuracy in predicting this kind of dip, however, does appear to require consideration of static deformation.

<u>Calculations for Flexible Wing</u>

When the wing is treated as flexible in the static-aeroelastic portion of the calculation procedure shown schematically in fig. 8, the "initial shape" input to the

"aeroelastic FLO22" iterative calculation of pressures and deformations may be the undeformed shape or, if available, a better approximation to the aeroelastically converged shape. If the latter is used, however, it is still necessary to input the undeformed shape ("jig" shape) of the wing into "aeroelastic FLO22" so that the calculated deformations may be added to it in order to obtain the output deformed shape and associated pressure distribution. Since jig-shape measurements for the TF-8A flutter-model wing were not available, a jig shape was calculated by subtracting from the design shape the deformations caused by the load distribution on the design shape at the design condition (M = 0.99, C_L = 0.37).

For the flexible wing the experimental flutter dynamic pressure was input to the static aeroelastic calculation (fig. 8), and a single pass was made through the computational sequence. Although the outer q-loop has not been closed at this time, the accuracy of the calculated results (triangle symbols in figs. 9(a) and (b)) is well indicated by comparison of the calculated and experimental flutter points. Since the experimental flutter dynamic pressure was input, perfect agreement between calculation and experiment would be indicated by the same flutter dynamic pressure being calculated in a single pass through the outer loop. It is evident in figs. 9(a) and (b), however, that the inclusion of structural flexibility in combination with FLO22 leads to excessively high flutter speeds. This result was not unanticipated.

For the higher Mach numbers and higher loading conditions potential-flow methods, including FLO22, characteristically produce shockwaves that are too strong and too far aft. Moreover, once the shock has moved aft, it exhibits very little further movement with changes in angle of attack or deformation and hence generates little further change in section lift-curve slopes and aerodynamic centers. Thus, for example, in the present calculations of loading (and hence deformation) at the design condition (M = 0.99, C_L = 0.37), calculated C_{L_0} was considerably higher and C_{L_α} was considerably lower than corresponding experimental values (from ref. 16). These aerodynamic deficiencies raise doubts concerning the accuracy of the calculated jig shape. In addition, the low values of calculated lift-curve slopes also contribute to the excesively high calculated flutter speeds shown in figs. 9(a) and (b).

In contrast, the wing in a physical (viscous) flow will experience shocks that are weaker and farther forward. Consequently, as flutter dynamic pressure decreases into the transonic dip, the flexible wing deforms less and less, the outer wing sections assume higher local angles of attack, as previously described, shocks strengthen and migrate aft, and the effective section lift-curve slopes increase. This effect of diminishing deformation thus contributes to a still lower flutter dynamic pressure. Since this behavior is not accurately obtained from FLO22, it is evident that, as expected, accurate flutter prediction will require the inclusion of viscous effects on shock strength and location. Static aeroelastic and flutter calculations are in progress with the FLO22 code replaced by the FLO30 code (full-potential, conservation-form, finite-volume code) (ref. 21), including a coupled boundary-layer code (ref. 22) in order to address the current deficiencies.

CONCLUDING REMARKS

Modified-strip-analysis flutter calculations have been made for a supercritical wing with high design Mach number using aerodynamic parameters obtained from the FLO22 full-potential-flow code for the design shape (rigid) and for the aeroelastically deformed wing at approximately the flutter dynamic pressure. The unconventional backward turn of the transonic flutter boundary found experimentally at nonzero angles of attack was also calculated with aerodynamic parameters for the rigid design shape and was shown to be caused by variations in mass ratio. Quantitative accuracy in predicting this kind of transonic dip, however, appears to require consideration of static aeroelastic deformation. Inadequacies of the full-potential code at the high subsonic Mach numbers involved led to excessively high calculated flutter speeds for the flexible wing resulting from (1) poor definition of jig shape from the design shape, and (2) low values of section lift-curve slopes and aftward locations of section aerodynamic centers (relative to experiments) caused by excessively aftward shock locations that changed little with changes in angle of attack. The present methodology is valid, but accurate flutter predictions will require the inclusion of viscous effects on shock strength and location, at least for the wing used in this study. Such calculations are in progress.

REFERENCES

1. Farmer, Moses G.; Hanson, Perry W.; and Wynne, Eleanor C.: Comparison of Supercritical and Conventional Wing Flutter Characteristics. NASA TM-72837, 1976.

2. McGrew, J. A.; Giesing, J. P.; Pearson, R. M.; Zuhurudding, K.; Schmidt, M. E.; and Kalman, T. P.: Supercritical Wing Flutter, AFFDL-TR-78-37, 1978.

3. Yates, E. Carson, Jr.; Wynne, Eleanor C.; Farmer, Moses G.; and Desmarais, Robert N.: Prediction of Transonic Flutter for a Supercritical Wing by Modified Strip Analysis. J. Aircraft, Vol. 19, No. 11, November 1982, pp 999-1004.

4. Houwink, R.; Kraan, A. N.; and Zwaan, R. J.: Wind-Tunnel Study of the Flutter Characteristics of a Supercritical Wing. J. Aircraft, Vol. 19, No. 5, May 1982, pp. 400-405.

5. Yates, E. Carson, Jr.; Wynne, Eleanor C.; and Farmer, Moses G.: Effects of Angle of Attack on Transonic Flutter of a Supercrictical Wing. <u>J. Aircraft</u>, Vol. 20, No. 10, October 1983, pp. 841-847.

6. Yates, E. Carson, Jr.: Calculation of Flutter Characteristics for Finite-Span Swept or Unswept Wings at Subsonic and Supersonic Speeds by a Modified Strip Analysis, NACA RM L57L10, 1958.

7. Yates, E. Carson, Jr.: Modified-Strip-Analysis Method for Predicting Wing Flutter at Subsonic to Hypersonic Speeds. <u>J. Aircraft</u>, Vol. 3, No. 1, January-February 1966, pp. 25-29.

8. Yates, E. Carson, Jr.: Use of Experimental Steady-Flow Aerodynamic Parameters in the Calculation of Flutter Characteristics for Finite-Span Swept or Unswept Wings at Subsonic, Transonic, and Supersonic Speeds, NASA TM X-183, 1959.

9. Yates, E. Carson, Jr.; and Bennett, Robert M.: Use of Aerodynamic Parameters from Nonlinear Theory in Modified-Strip-Analysis Flutter Calculations for Finite-Span Wings at Supersonic Speeds, NASA TN D-1824, 1963.

10. Yates, E. Carson, Jr.: Subsonic and Supersonic Flutter Analysis of a Highly Tapered Swept-Wing Planform, Including Effects of Density Variation and Finite Wing Thickness, and Comparison with Experiments. NASA TN D-4230, 1967.

11. Yates, E. Carson, Jr.; and Bennett, Robert M.: Analysis of Supersonic-Hypersonic Flutter of Lifting Surfaces at Angle of Attack. <u>J. Aircraft</u>, Vol. 9, No. 7, July 1972, pp. 481-489.

12. Yates, E. Carson, Jr.: Flutter and Unsteady-Lift Theory. In "Performance and Dynamics of Aerospace Vehicles." NASA SP-258, 1971.

13. Jameson, A.; and Caughey, D. A.: Numerical Calculation of the Transonic Flow Past a Swept Wing, NASA CR-153297, 1977.

14. Theodorsen, Theodore: General Theory of Aerodynamic Instability and the Mechanism of Flutter. NACA Rep. 496, 1935.

15. Jordan, P. F.: Aerodynamic Flutter Coefficients for Subsonic, Sonic and Supersonic Flow (Linear Two-Dimensional Theory). R. & M. No. 2932, British A.R.C., 1957.

16. Harris, Charles D.: Wind-Tunnel Investigation of the Aerodynamic Load Distribution of a Supercritical Wing Research Airplane Configuration. NASA TM X-2469, 1972.

17. Persoon, A. J.; Horsten, J. J.; and Meijer, J. J.: Measurement of Transonic Dips in the Flutter Boundaries of a Supercritical Wing in a Wind Tunnel. <u>J. Aircraft</u>, Vol 21, No. 11, November 1984, pp. 906-912.

18. Sandford, Maynard C.; Ruhlin, Charles L.; and Abel, Irving: Flutter Studies of Simplified Component Models of a Variable-Sweep-Wing Airplane at Mach Numbers Up to 3.0. NASA TN D-3501, 1966.

19. Desmarais, Robert N.; and Bennett, Robert M.: User's Guide for a Modular Flutter Analysis Software System (FAST Version 1.0). NASA TM 78720, 1978.

20. Whitlow, Woodrow, Jr.; and Bennett, Robert M.: Application of a Transonic Potential Flow Code to the Static Aeroelastic Analysis of Three-Dimensional Wings. AIAA Paper No. 82-0689, 1982.

21. Caughey, D. A.; and Jameson, Antony: Progress in Finite-Volume Calculations for Wing-Fuselage Combinations. <u>AIAA Journal</u>, Vol. 18, November 1980, pp. 1281-1288.

22. Streett, C. L.: Viscous-Inviscid Interaction for Transonic Wing-Body Configurations Including Wake Effects. <u>AIAA Journal</u>, Vol. 20, No. 7, July 1982, pp. 915-923.
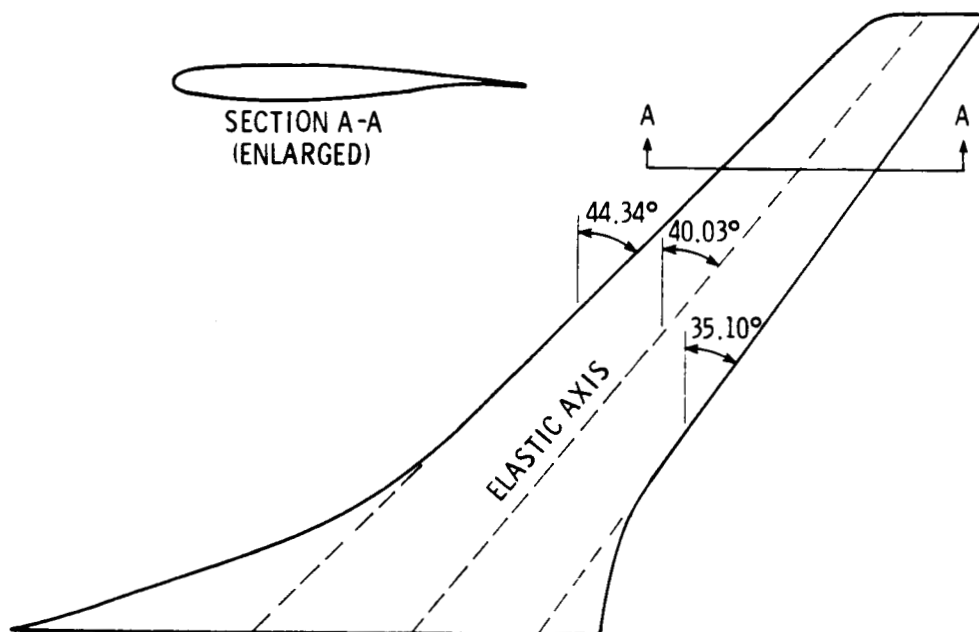
SECTION A-A
(ENLARGED)

ELASTIC AXIS

44.34° 40.03°

35.10°

A   A

Fig. 1 - Supercritical wing flutter model

SOLID SYMBOLS INDICATE LOW DAMPING
—O— FLUTTER EXPERIMENT
—□— AERO. PARAMETERS FROM 8-FOOT TUNNEL

$$\frac{V}{b_r \omega_r \sqrt{\mu_r}}$$
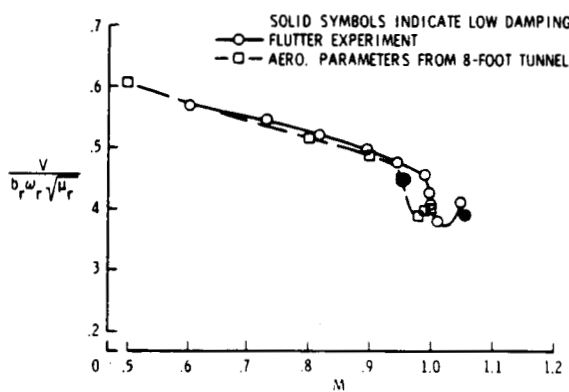
O FLUTTER EXPERIMENT
● LOW DAMPING

μ_r

Fig. 2 - Experimental and calculated
flutter in Freon-12 at $\alpha = 0$
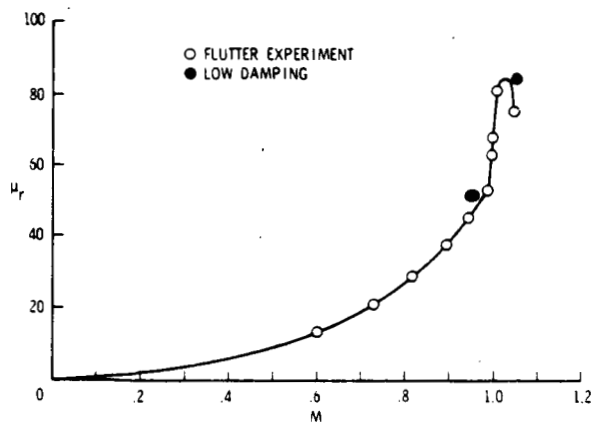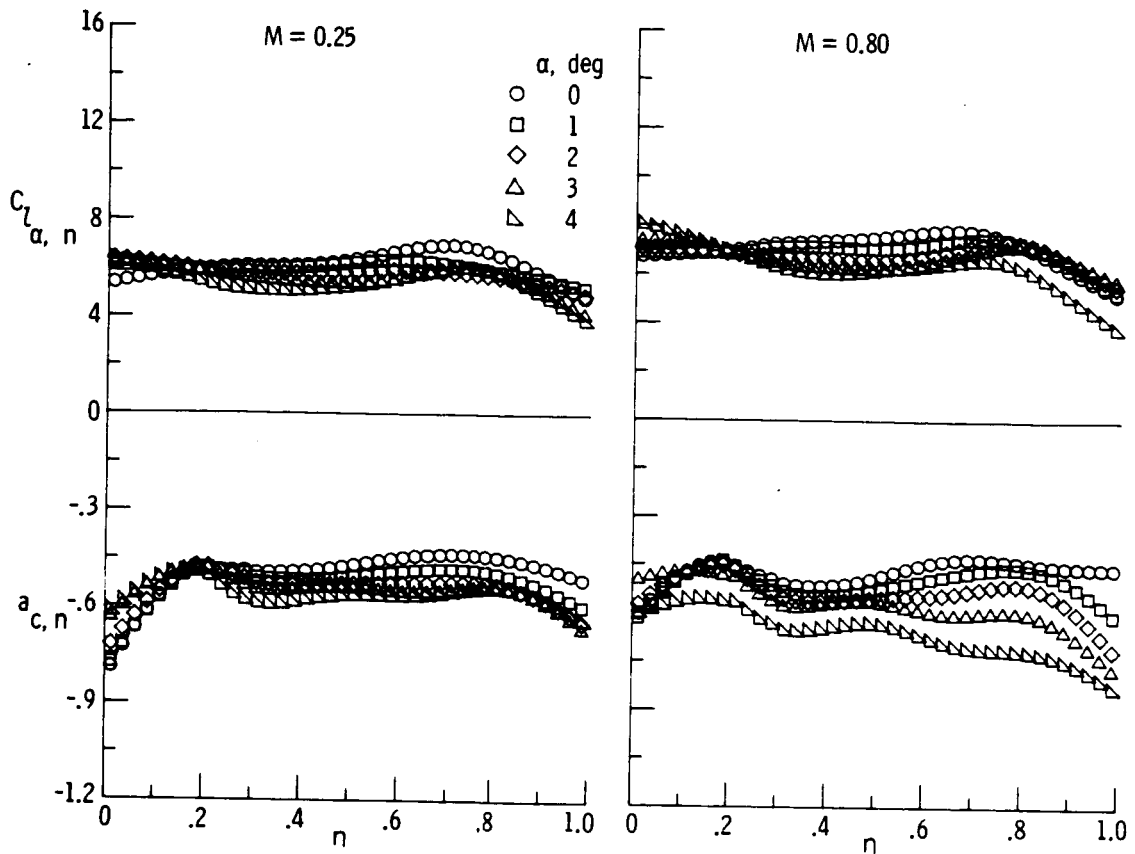
Fig. 3 - Mass ratios for flutter
experiments in Freon-12

8

Fig. 4 - Typical aerodynamic parameters for flutter analysis at subsonic Mach numbers
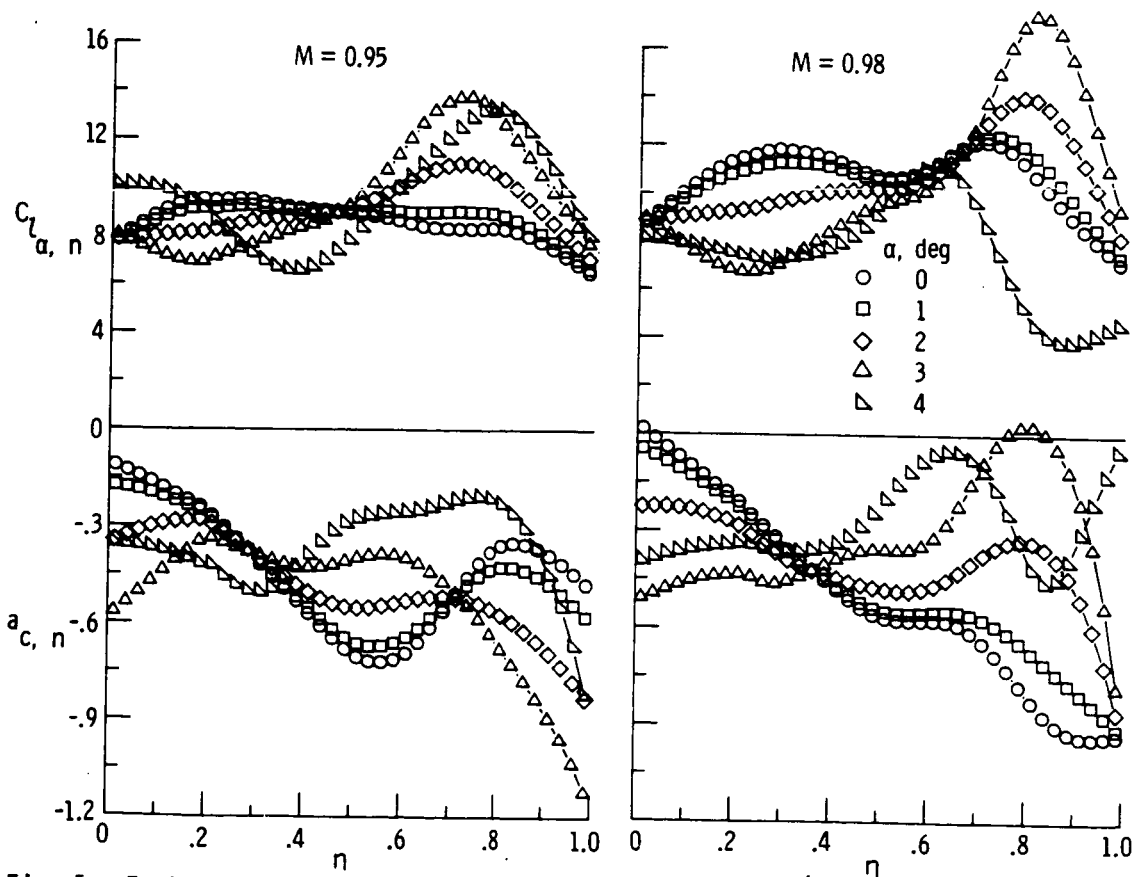
Fig. 5 - Typical aerodynamic parameters for flutter analysis at transonic Mach numbers

9
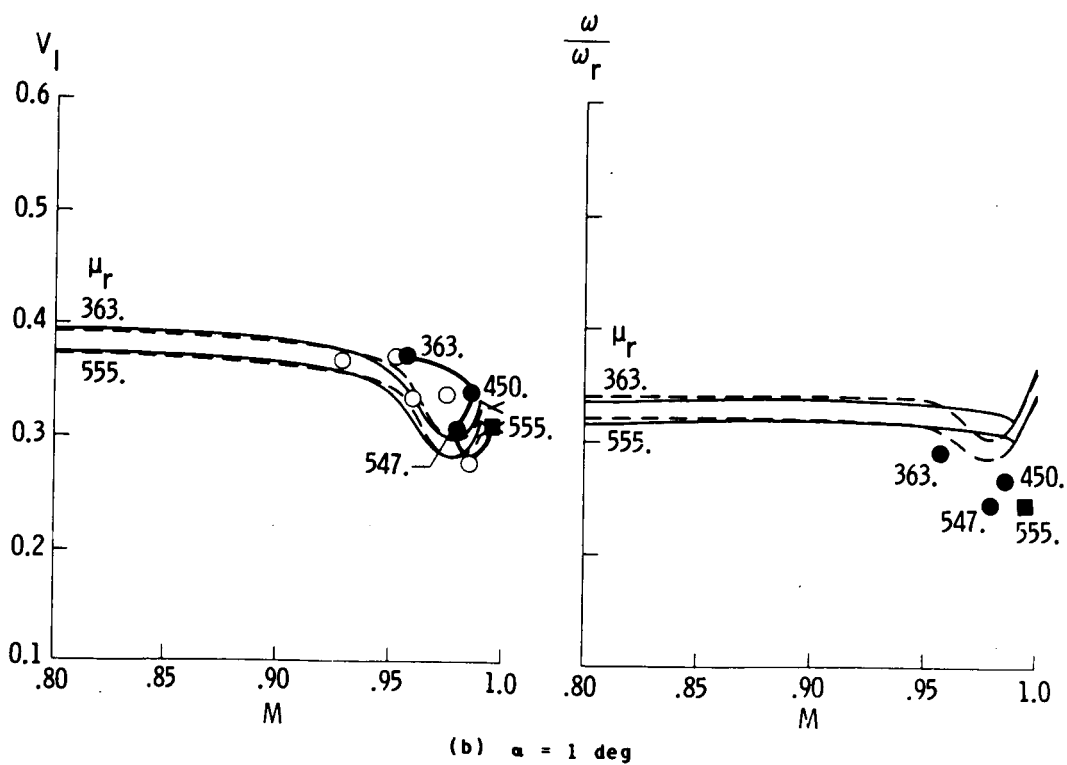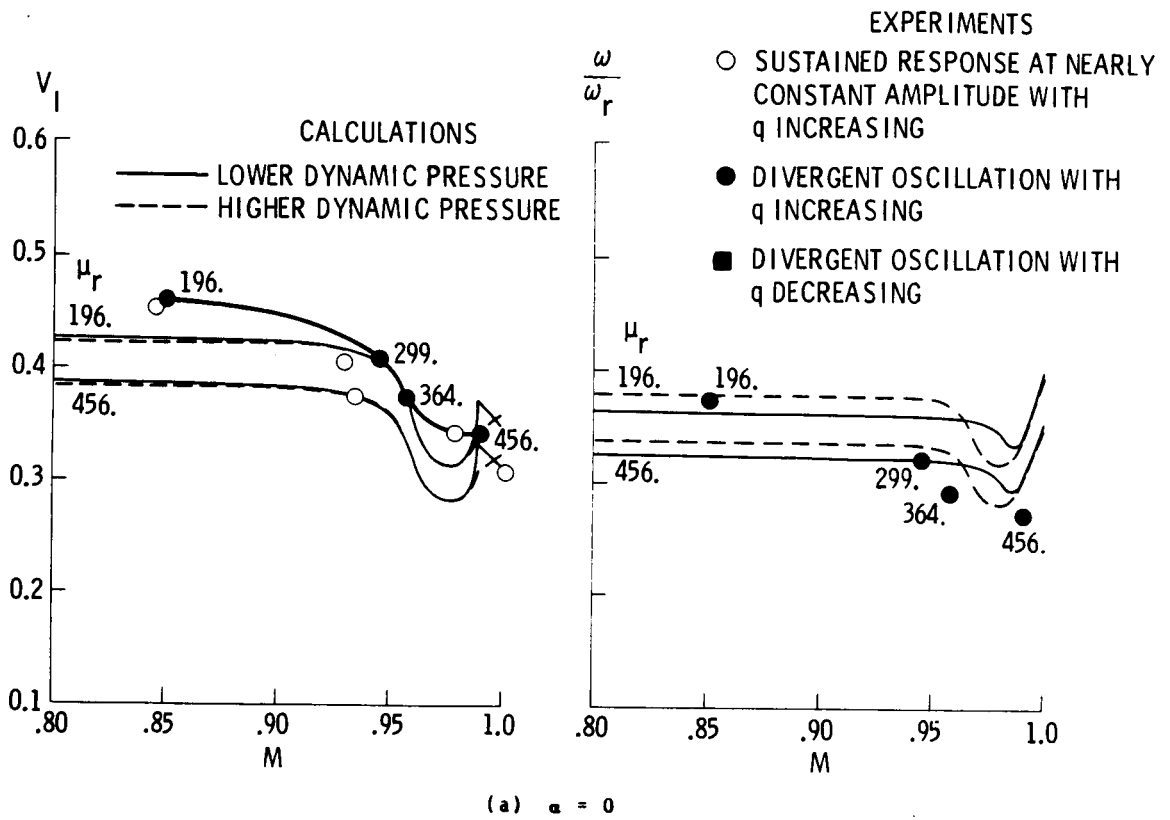
Fig. 6 - Flutter in air obtained from experiments and from calculations with experimental aerodynamic parameters

10

(c) α = 2 deg
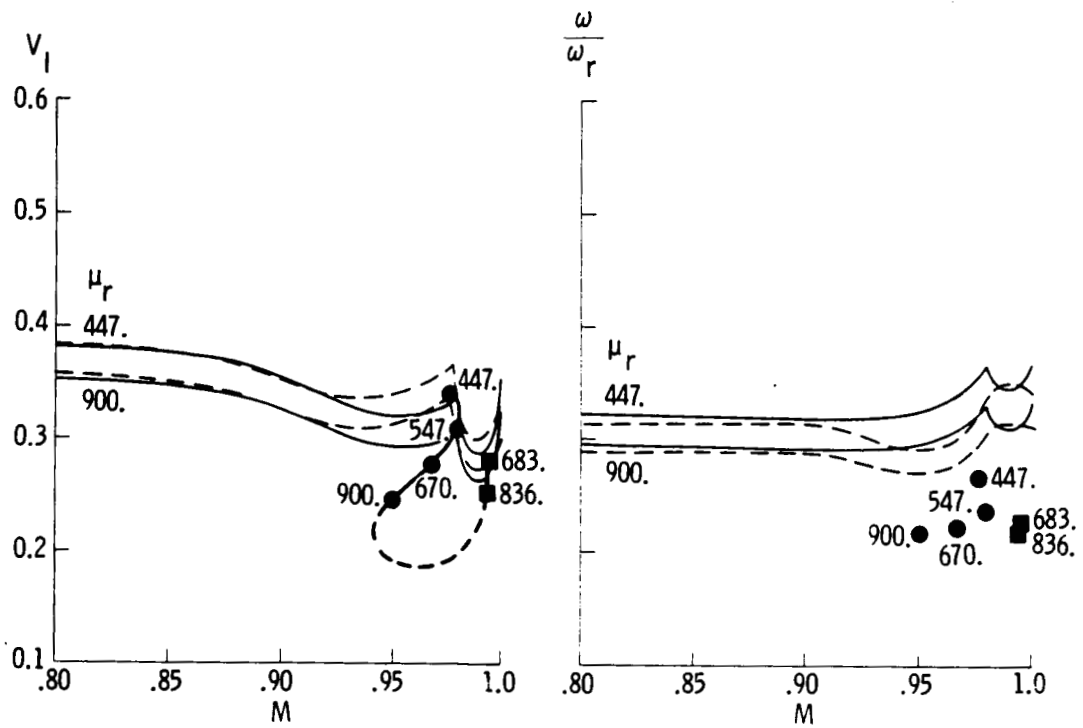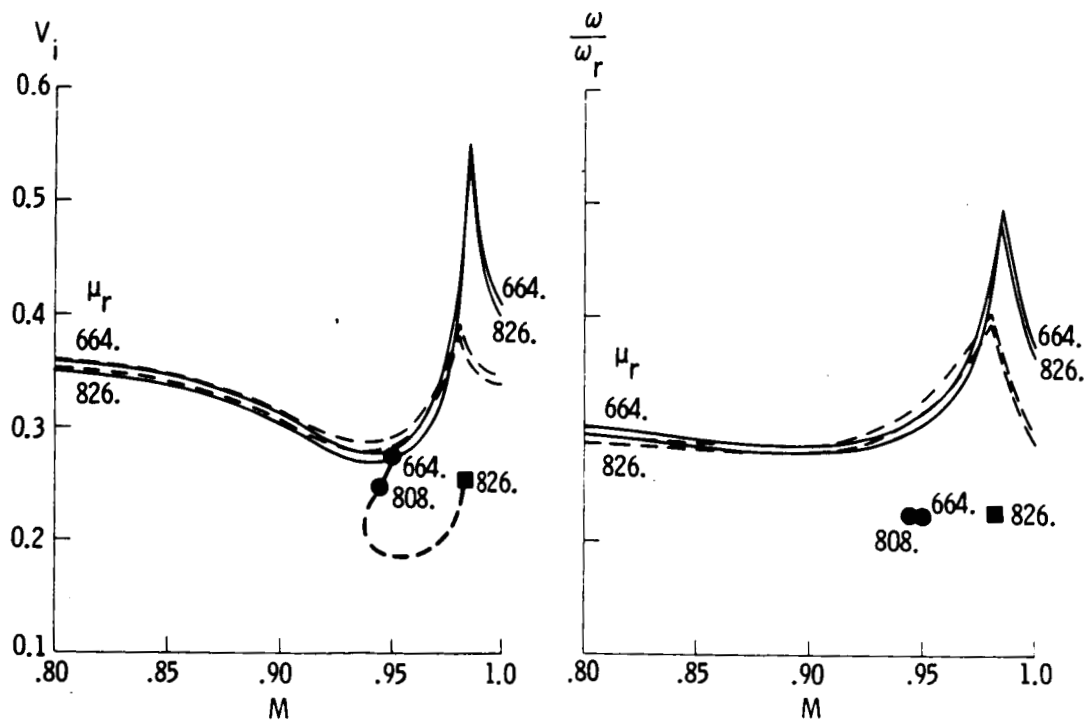
(d) α = 3 deg

Fig. 6 - Concluded
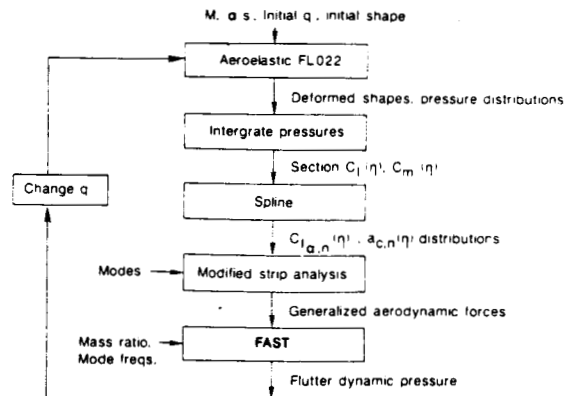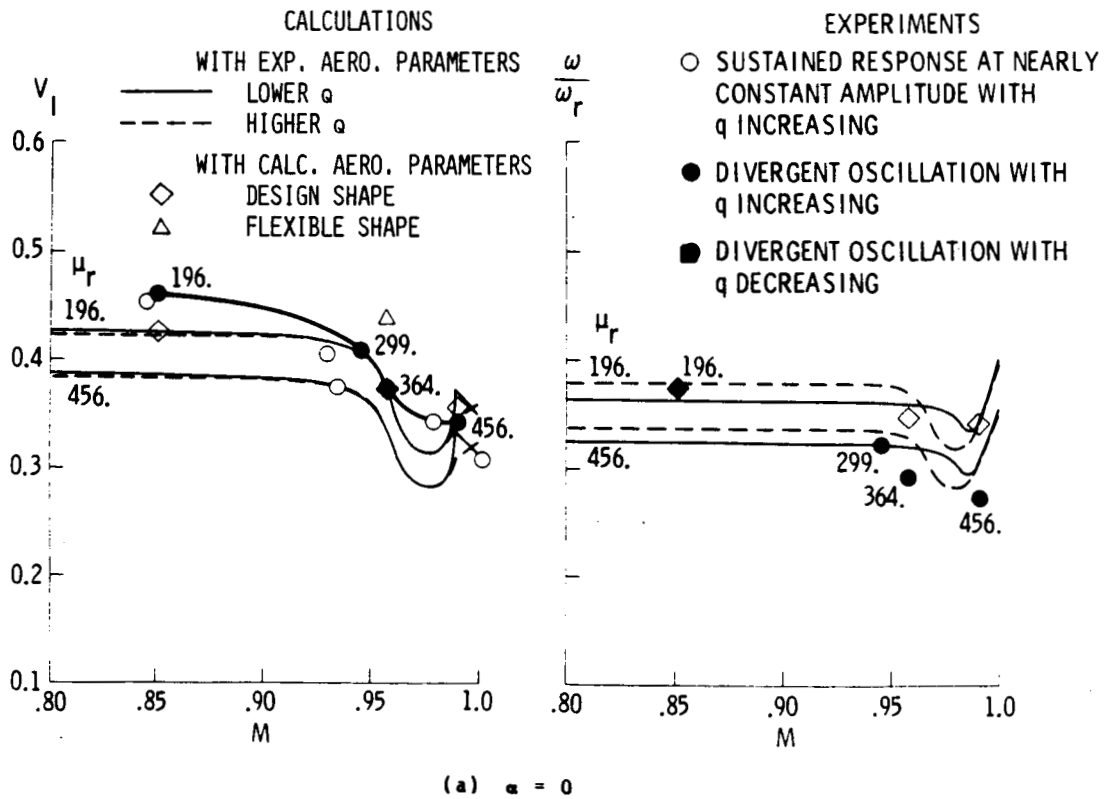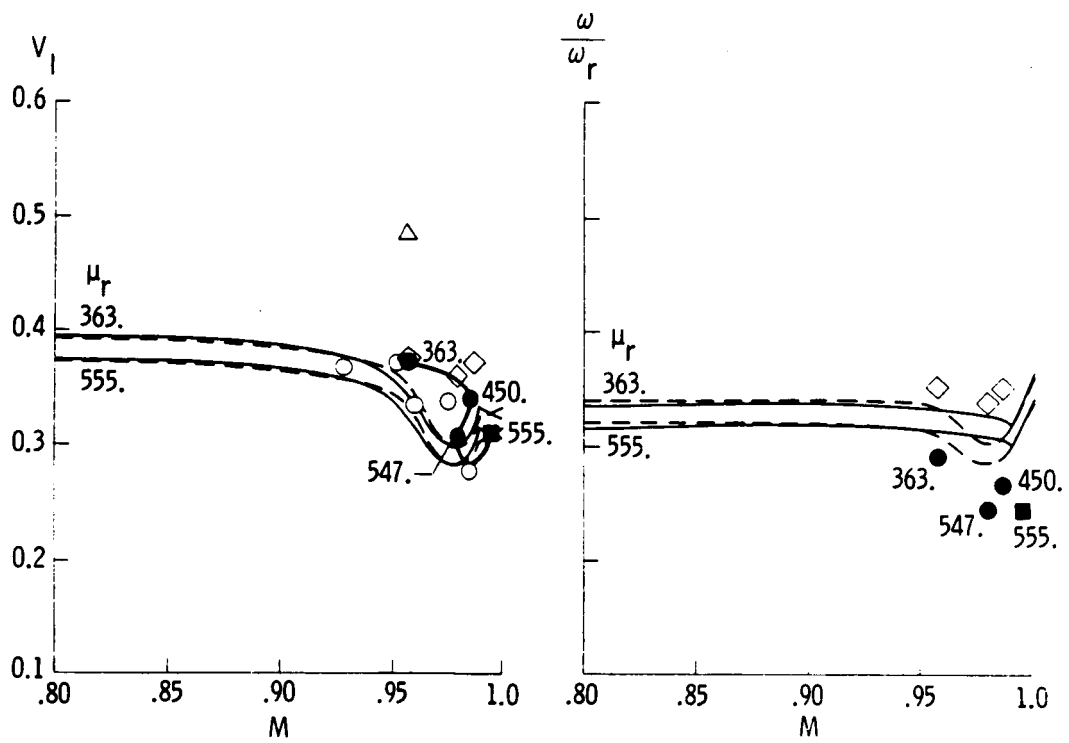
11
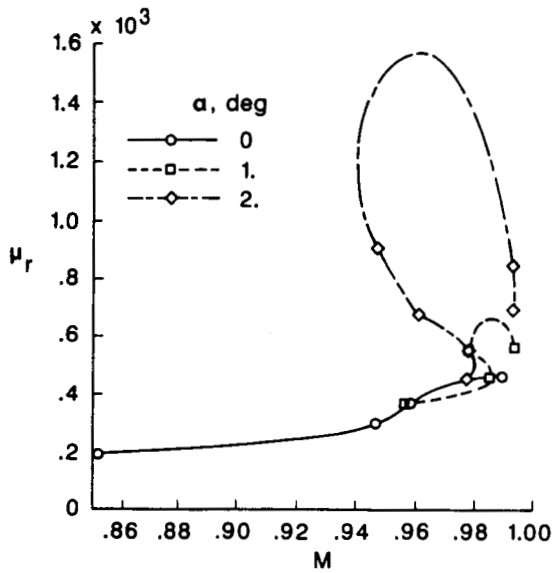
Fig. 7 - Mass ratios for flutter
experiments in air

Fig. 8 - Matched static-aeroelastic
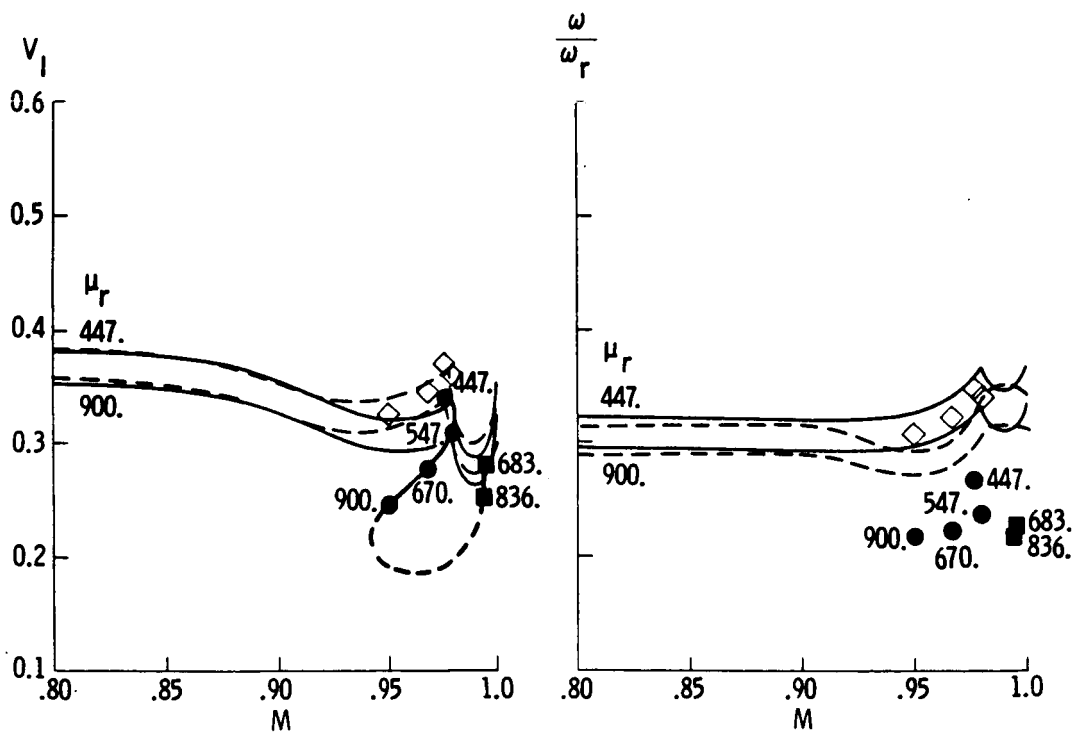and flutter calculations

(a) α = 0

Fig. 9 - Flutter in air obtained from calculations with calculated aerodynamic parameters
and comparison with previous results

12

(b) α = 1 deg

Fig. 9 - Continued
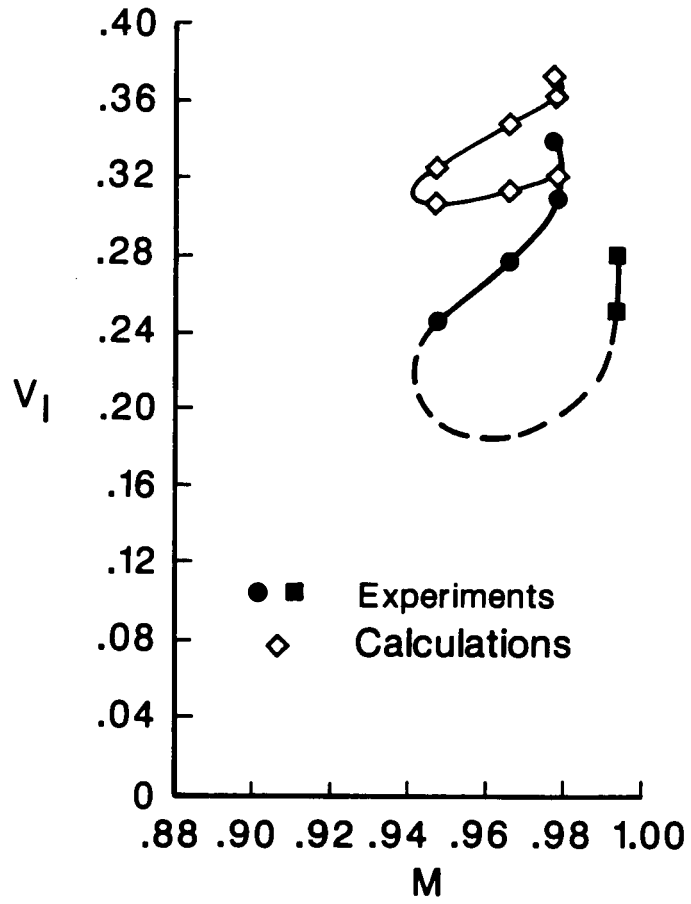

(c) α = 2 deg

Fig. 9 - Concluded

13

Fig. 10 - Transonic dip from flutter experiments and from calculations with calculated
aerodynamic parameters for design shape and mass ratios from fig. 7; α = 2 deg

1. Report No. NASA TM-89132	2. Government Accession No.	3. Recipient's Catalog No.
4. Title and Subtitle Static Aeroelastic Effects on the Flutter of a Supercritical Wing		5. Report Date March 1987
		6. Performing Organization Code
7. Author(s) E. Carson Yates, Jr.; Li-Chuan Chu		8. Performing Organization Report No.
9. Performing Organization Name and Address NASA Langley Research Center Hampton, Va 23665-5225		10. Work Unit No. 505-63-21
		11. Contract or Grant No.
12. Sponsoring Agency Name and Address National Aeronautics and Space Administration Washington, DC 20546-0001		13. Type of Report and Period Covered Technical Memorandum
		14. Sponsoring Agency Code

16. Abstract

It is well known that wings with supercritical airfoils generally have lower transonic flutter speeds than similar wings with conventional airfoils and that small increases in angle of attack from zero and the accompanying static aeroelastic deformations have further detrimental effects on transonic flutter. This paper presents the results of an effort to calculate the effects of angle of attack and the associated aeroelastic deformation on the flutter of a highly swept supercritical wing by use of the modified strip analysis employed in previous studies of this wing. The spanwise distributions of steady-state section lift-curve slope and aerodynamic center required as input for these calculations were obtained from static aeroelastic calculations for the wing by use of the FLO22 transonic code and an assumed dynamic pressure. The process is iterative so that flutter can be obtained at the same dynamic pressure as that used to calculate the statically deformed shape and loading about which the flutter oscillation occurs (matched conditions). The results of this investigation show that the unconventional backward turn of the transonic dip in the experimental flutter boundary for angles of attack greater than zero is caused by variations in mass ratio and not by static aeroelastic deformation, although inclusion of the latter appears to be required for quantitative accuracy in the calculations. For the very high subsonic Mach numbers of this investigation, however, quantitative accuracy will also require inclusion of viscous effects on shock strength and location.

17. Key Words (Suggested by Author(s)) Aeroelasticity Flutter Supercritical Wings	18. Distribution Statement Unclassified - Unlimited Subject Category 39		
19. Security Classif. (of this report) Unclassified	20. Security Classif. (of this page) Unclassified	21. No. of Pages 15	22. Price A02